

MATERIALS SCIENCE

Highly efficient and stable deep-blue organic light-emitting diode using phosphor-sensitized thermally activated delayed fluorescence

Eungdo Kim¹, Junha Park¹, Mieun Jun¹, Hyosup Shin¹, Jangyeol Baek¹, Taeil Kim¹, Seran Kim¹, Jiyong Lee¹, Heechoon Ahn¹, Jinwon Sun¹, Soo-Byung Ko¹, Seok-Hwan Hwang¹, Jun Yeob Lee², Changwoong Chu^{1*}, Sunghan Kim^{1*}

Phosphorescent and thermally activated delayed fluorescence (TADF) blue organic light-emitting diodes (OLEDs) have been developed to overcome the low efficiency of fluorescent OLEDs. However, device instability, originating from triplet excitons and polarons, limits blue OLED applications. Here, we develop a phosphor-sensitized TADF emission system with TADF emitters to achieve high efficiency and long operational lifetime. Peripheral carbazole moieties are introduced in conventional multi-resonance-type emitters containing one boron atom. The triplet exciton density of the TADF emitter is reduced by facilitating reverse intersystem crossing, and the Förster resonant energy transfer rate from phosphor sensitizer is enhanced by high absorption coefficient of the emitters. The emitter exhibited an operational lifetime of 72.9 hours with Commission Internationale de L'Eclairage chromaticity coordinate $y=0.165$, which was 6.6 times longer than those of devices using conventional TADF emitters.

INTRODUCTION

Thermally activated delayed fluorescence (TADF) (1–2) and phosphorescent (3–5) organic light-emitting diodes (OLEDs) have been developed as candidates of next-generation blue OLEDs and as alternatives to fluorescent OLEDs having low external quantum efficiencies (EQEs). In the TADF mechanism, organic molecules absorb thermal energy to transform nonemissive triplet excited states (T_1) into singlet excited states (S_1) that can radiatively relax to the ground state. Here, the energy gap between the lowest S_1 and the lowest T_1 (ΔE_{ST}) must be minimized for efficient emission (should be <0.2 eV). A small energy gap is achieved by spacing spatially separated and twisted donor and acceptor moieties. In addition, strong vibronic coupling between T_1 and T_n ($n > 1$) as well as high spin-orbit coupling between singlet and triplet states is required (6–8). Donor-acceptor (D-A)-type blue TADF materials have been developed, owing to their design versatility and relatively short delayed fluorescence lifetime (~ 1 μ s) (9–10). However, D-A-type blue TADF emitters are unsuitable to develop commercialized top-emitting OLEDs requiring narrow emission spectra (11–12). To overcome this problem, recently developed boron-derived multiple resonance (MR)-type TADF emitters (13–19) could be considered promising candidates of narrow-emitting materials owing to their more rigid chemical structures than those of D-A-type TADF emitters. They are suitable replacements for fluorescent emitters as they exhibit a color coordinate of full width at half maximum (FWHM) < 20 nm and high EQE $> 15\%$; however, they demonstrate poor device stability owing to long-lived excitons having high-energy triplet state.

To achieve long device lifetime with high efficiency, a device structure that harvests triplet excitons using a sensitizer was proposed

(20–21). To date, all studies have focused on sensitizers rather than the final TADF emitters, neglecting the characteristics of the final emitters that substantially affect device performance. Only the well-known *t*-DABNA (2,12-di-*tert*-butyl-5,9-bis(4-(*tert*-butyl)phenyl)-5,9-dihydro-5,9-diaza-13b-boranaphtho[3,2,1-de]anthracene) and *v*-DABNA (N7,N7,N13,N13,5,9,11,15-octaphenyl-5,9,11,15-tetrahydro-5,9,11,15-tetraaza-19b,20b-diboradinaphtho[3,2,1-de:1',2',3'-jk]pentacene-7,13-diamine) have been used without any emitter modifications for the triplet exciton harvesting the TADF system (22–31). *t*-DABNA has a suitable light emission spectrum for application as pure blue OLEDs; however, they exhibit a relatively short device lifetime. Although *v*-DABNA has a longer device lifetime than *t*-DABNA, it cannot achieve pure-blue emission owing to its red-shifted peak wavelength. Therefore, further studies on the MR-type TADF emitter for the singlet exciton-harvesting TADF OLED are essential.

Developing a well-arranged device architecture is necessary to simultaneously achieve high efficiency and long device lifetime in deep-blue OLEDs using TADF emitters. Because both high-energy and long-lived triplet excitons and polarons in TADF emitters generally decrease device lifetime and EQE, controlling their quantities is essential for achieving high performance of the OLEDs. Recently, phosphor-sensitized TADF (PST) systems have been developed, which use an efficient TADF blue emitter (TBE) combined with phosphor sensitizer (PS) (22). The emission path is roughly divided into two processes: Prompt decay emission stems from singlet state emitter transferred from the PS and delayed decay emission from excitons up-converted from inevitably populated triplet states in the emitter. The efficient and stable blue emitter is one of the most important factors for a high-performance blue PST system.

Therefore, here, we report novel MR-type TADF emitters to achieve high efficiency and long device lifetime of deep-blue OLEDs. Peripheral carbazoles are introduced into the emitter to reduce triplet exciton and trapped charge within emissive layer (EML). The carbazole derivatized emitter is expected to have mitigating effects in terms of triplet and polaron-related device degradation. The

Copyright © 2022 The Authors, some rights reserved; exclusive licensee American Association for the Advancement of Science. No claim to original U.S. Government Works. Distributed under a Creative Commons Attribution NonCommercial License 4.0 (CC BY-NC).

¹Materials Research Team, Display Research Center, Samsung Display, Giheung, Gyeonggi 17113, Republic of Korea. ²School of Chemical Engineering, Sungkyunkwan University, Suwon, Gyeonggi 16419, Republic of Korea.

*Corresponding author. Email: shan0819.kim@samsung.com (S.K.); changwoong.chu@samsung.com (C.C.)

emitters exhibit high molar extinction coefficient, fast reverse intersystem crossing, and weak hole trapping characteristics. In addition, bulky peripheral derivatives can suppress Dexter energy transfer from nearby molecules such as sensitizer and host to the emitter. PST devices made with this emitter show 6.6 times longer device lifetimes than that of systems using the conventional TADF emitter in bottom-emitting devices (24). Moreover, five times enhancement in device lifetime with 25.5 cd A^{-1} is observed in top-emitting devices. To our best knowledge, the highest reported top-emissive device performances were obtained.

RESULTS

Molecule design and photophysical properties

Our TADF molecular design strategy for the PST system was intended to mainly achieve high color purity, high efficiency, and long operational lifetime by facilitating Förster energy transfer (32–33) and suppressing Dexter energy transfer from the exciplex host and PS to the TBEs. This is because the increase in the number of relatively long-lived triplet excitons on the TADF emitter decreases the device stability and generates a large efficiency roll-off by deactivation processes, such as triplet-triplet annihilation (TTA) and singlet-triplet annihilation (STA) (34). To verify our concept, we designed MR-type TADF emitters having narrow FWHM, high photoluminescence quantum yield (PLQY), and small Stokes' shift. These emitters are required to meet four conditions: (i) The highest occupied molecular orbital (HOMO) energy difference between emitter and the host (or PS) should be minimized to reduce the number of triplet excitons and polarons on the TADF emitter generated by direct hole trapping. (ii) Sufficiently large molar extinction coefficient of the emitter is required for efficient Förster energy transfer through a large spectral overlap between the TBE and PS. (iii) They must exhibit small singlet-triplet splitting energy (ΔE_{ST}) and high spinning-orbit coupling constant to facilitate reverse intersystem crossing from the triplet to S_1 (35–37). (iv) Dexter energy transfer (38–39) from host and sensitizer should be blocked to minimize loss path through triplet state. Boron-based MR-type TADF emitters bearing peripheral electron-donating carbazole moieties (TBE01 and TBE02) were found to meet these requirements and were thus synthesized as shown in Fig. 1A (see also fig. S1). For comparison, *t*-DABNA, the well-known MR-type TADF emitter in the sensitizing system, was prepared. The chemical structures of these emitters were identified

by ^1H and ^{13}C nuclear magnetic resonance (NMR) spectroscopy (figs. S2 to S9).

To gain insight into the geometrical and electronic properties of TADF emitter at the molecular level, the HOMO and the lowest unoccupied molecular orbital (LUMO) were calculated with time-dependent density functional theory (TDDFT) and the B3LYP/6-311G** method, which provide an orbital interpretation of locally excited transition. As shown in Fig. 1 (B and C), the frontier orbitals of the TADF molecules consisting of rigid polycyclic aromatic framework are efficiently separated by the MR effects of the nitrogen and boron atoms. This obvious spatial separation of the frontier orbitals of the newly designed emitters afforded smaller calculated ΔE_{ST} values than that of *t*-DABNA (*t*-DABNA, TBE01, and TBE02 have ΔE_{ST} values of 0.47, 0.44, and 0.42 eV, respectively; table S1), allowing for an efficient RNA-induced silencing complex. In addition, the large oscillator strengths of the S_0 - S_1 transition of the emitters can lead to large molar extinction coefficients (*t*-DABNA, TBE01, and TBE02 have molar extinction coefficients of 0.22, 0.30, and 0.44 eV, respectively; table S2), enabling efficient energy transfer between PS and TADF emitter.

The ultraviolet-visible (UV-vis) absorption and photoluminescent (PL) spectra of the emitters (TBE01 and TBE02) are shown in fig. S10. Both TBE01 and TBE02 show major absorption peaks at 447 nm, which is attributable to the short-range charge transfer transition from the B-N-containing core. The broad absorption band assigned to the π - π^* transition in the peripheral carbazole moieties is also clearly observed in the high-absorbance regions (300 to 350 nm). Moreover, the molar extinction coefficient of the emitters gradually increases with the increasing peripheral carbazole moieties in the order of TBE02 ($5.6 \times 10^4 \text{ M}^{-1} \text{ cm}^{-1}$) > TBE01 ($3.9 \times 10^4 \text{ M}^{-1} \text{ cm}^{-1}$) > *t*-DABNA ($2.3 \times 10^4 \text{ M}^{-1} \text{ cm}^{-1}$) (fig. S11). The optical bandgaps (E_g) of TBE01, TBE02, and *t*-DABNA, as determined from the absorption onset wavelength, were estimated to be very similar and were approximately 2.68, 2.68, and 2.70 eV, respectively. Upon excitation at 342 nm, the PL spectra of TBE01 and TBE02 at 298 K display intense deep-blue emissions centered at 459 nm with a bathochromic shift of ~ 3 nm, compared to that of *t*-DABNA. As expected, both TBE01 and TBE02 exhibit extremely small Stokes' shift of 12 nm and a narrow FWHM of 21 nm, resulting from the reduced vibronic coupling and the suppressed vibrational relaxation in the rigid boron-based MR-type TADF emitter. In contrast, at the sub- E_{HOMO} levels, the resonance-donating effect of the carbazole group is dominant,

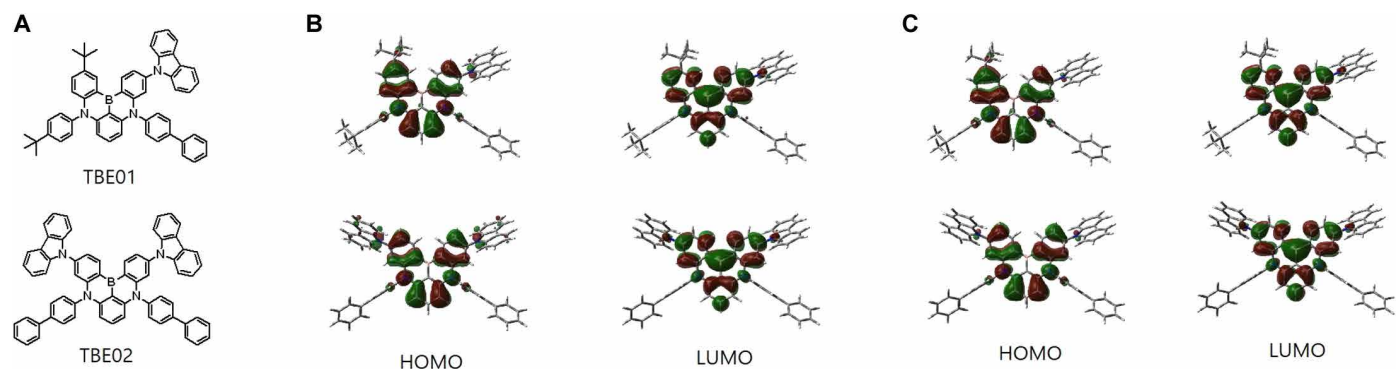


Fig. 1. Molecular structures and frontier molecular orbitals. (A) Molecular structures of TBE01 and TBE02. (B) Calculation result of the energies of the HOMO/LUMO singlet orbitals of TBE01 and TBE02. (C) Calculated triplet spin density distributions of the lowest excited triplet states of TBE01 and TBE02.

and the level is shallower than that where the effect is weak. In particular, TBE02 shows a resonance-donating effect up to the $E_{\text{HOMO}-2}$ level because more carbazole moieties are introduced than those in TBE01. Owing to the shallowly formed $E_{\text{HOMO}-n}$ level, the electron transition from the sub- E_{HOMO} level to the LUMO level could be facilitated (table S2 and figs. S12 and S13).

The low-temperature photoluminescence spectra obtained at 77 K were used to determine the triplet energies (E_{T}) of TBE01 and TBE02 (fig. S10). Considering that the highest-energy phosphorescence peak corresponds to the $T_1 \rightarrow S_0$ transition, the E_{T} values of the two emitters were estimated to be ~ 2.54 and 2.56 eV, respectively. The ΔE_{ST} values of TBE01 and TBE02 (~ 0.16 and 0.14 eV, respectively) were slightly smaller than that of *t*-DABNA (0.21 eV). Moreover, TBE01 and TBE02 show rather high PLQYs of 91.1 and 89.1%, respectively (Table 1). This may be as a result of the reduced exchange energy between the S_1 and T_1 states by the more extended π -conjugate system and the improved radiative recombination by the increased oscillation strength (f value) based on the effect of the peripheral electron-donating carbazole moieties. Förster radius from the sensitizer to the emitters are calculated to be 4.5, 4.2, and 3.7 nm for TBE02, TBE01, and *t*-DABNA, respectively (random orientation is assumed for simplicity). The photophysical characteristics of PS, Platinum(II) [2-[3-[3-[3,5-bis(1,1-dimethylethyl)phenyl]-1H-benzimidazol-1-yl- κ C2]phenoxy- κ C2]-9-[4-(1,1-dimethylethyl)-2-pyridinyl- κ N]-9H-carbazolato(4-)- κ C1] (PtON-TBBI), examined here is summarized in fig. S14 and table S3.

Figure 2A shows the PL decay curves of TBE doped onto the exciplex host materials. The decay curves indicate the typical TADF emission process because the curve is clearly separated into a distinctive, prompt, and delayed emission component. The rISC rate constant (k_{rISC}) from the triplet to S_1 of the emitters are 0.27×10^4 ,

0.51×10^4 , and 1.03×10^4 s^{-1} for *t*-DABNA, TBE01, and TBE02, respectively (table S4). The k_{rISC} value substantially increased upon the addition of peripheral carbazole moieties. The high k_{rISC} of TBE02 might be ascribed to the smaller ΔE_{ST} compared with those in *t*-DABNA and TBE01. Furthermore, we investigated the transient PL decay curves of the films wherein the PS and TBE are codeposited into exciplex host material (Fig. 2B). The efficient Förster energy transfer from triplet state of the sensitizer to singlet state of the emitter decreases the decay time of the PST system, while Dexter energy transfer increases the decay time of the system (22, 29). Dexter energy transfer increases the number of the triplet exciton in the emitter after the transfer, which results in a slow deactivation of the excited states as the depopulation of the triplet excitons on the TADF emitter occurs mainly via uphill reverse intersystem crossing. This suggests that the emission decay time of the phosphor-sensitized TBE could be substantially shorter than that of the TBE without PS if Förster energy transfer is efficient (40). TBE02 displays the shortest decay time as shown in Fig. 2B because TBE02 allows the most efficient Förster energy transfer and the highest k_{rISC} among the emitters examined here. Intensity-averaged decay time of *t*-DABNA, TBE01, and TBE02 in this PST system are 11.2, 9.3, and 7.2 μs , respectively. The decreased decay time is advantageous because it contributes to the reduction in the exciton concentration and the concomitant improvement of the operational lifetime of the device (41). To study the structure-property relationship in the energy transfer system, TDDFT calculations for the lowest excited triplet state were performed. As shown in Fig. 1C, triplet spin density distribution of TBE is mainly localized on the B-N core. The terminal substituents, such as carbazole, biphenyl, and *t*-butyl (42), not only increase intermolecular distance between TADF emitter and the neighboring molecules but also reduce their orbital overlaps (20). Carbazole moiety of length 6.84 nm

Table 1. Photophysical and electrochemical properties of the emitters (*t*-DABNA, TBE01, and TBE02).

Compound	λ_{abs}^* (nm)	$\lambda_{\text{em}}^\dagger$ (nm)	FWHM [†] (nm)	PLQY [‡] (%)	ΔE_{ST} (eV)	E_{g}^{\S} (eV)	$E_{\text{HOMO}}^{\parallel}$ (eV)	$E_{\text{LUMO}}^{\parallel}$ (eV)
<i>t</i> -DABNA	444	456	21	99.3	0.21	2.70	-5.12	-2.42
TBE01	447	459	21	91.1	0.16	2.68	-5.21	-2.53
TBE02	447	459	21	89.1	0.14	2.68	-5.29	-2.61

*Measured in dilute toluene solution (1.0×10^{-5} M). †Measured in dilute toluene solution (1.0×10^{-6} M). ‡Measured in dilute toluene solution under nitrogen (1.0×10^{-3} M). §Estimated from the absorption edge. ||Measured from DPV scanning. ¶Estimated from HOMO and bandgap (E_{g}) energies.

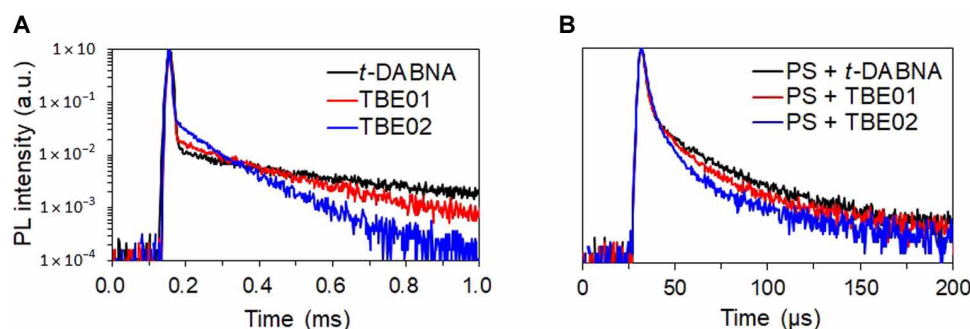


Fig. 2. Transient PL decay profiles. (A) *t*-DABNA, TBE01, and TBE02 (0.4 wt %) doped on the SiCzCz:SiTrzCz2 host films. (B) PS (13 wt %) was codeposited with 0.4 wt % emitter in the SiCzCz:SiTrzCz2 host films. Mixing ratio of HT to ET host was 6.5:3.5. a.u., arbitrary units.

can help avoid intermolecular Dexter energy transfer as the Dexter energy transfer decreases exponentially with distance between donor and acceptor.

The electrochemical behaviors of TBE01 and TBE02 were investigated (fig. S15) by differential pulse voltammetry (DPV). Because nitrogen has higher electronegativity than carbon (although carbazole is generally an electron-donating group), it will withdraw more electrons from the B-N-containing core, leading to deeper HOMO levels in TBE01 and TBE02 (43). Considering the oxidation peak potential, the HOMO levels were measured to be approximately -5.21 and -5.29 eV, respectively, which were deeper than those of *t*-DABNA (Table 1). We compared the current density and voltage in the hole-only devices for the three TBEs. The EML of the devices comprised the exciplex host and TBE. The current density of the devices increases as the HOMO level of the TBEs decreases, as shown in Fig. 3. The TBE with a deeper HOMO level, corresponding to a shallower trap energy, resulted in a higher current density at the same applied voltage. Direct hole trapping into the emitters would be decreased for TBE01 and TBE02 because HOMO energy difference between emitter and host is decreased from 0.38 eV for *t*-DABNA to 0.29 and 0.26 eV for TBE01 and TBE02, respectively (Fig. 4). Therefore, the increased current density of the device with TBE02 represents the less-effective direct hole trapping on TBE02, compared to that on other TBEs. The direct charge trapping by the TBEs could increase

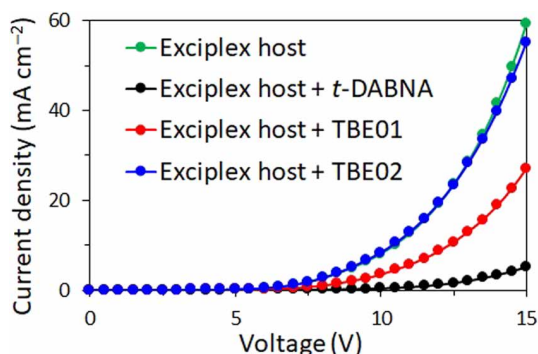


Fig. 3. Current-voltage profiles of the hole-only devices. The fabricated hole-only devices have a structure of ITO/BCFN + HAT-CN/BCFN/SiCzCz/SiCzCz:SiTrzCz2 (6.5:3.5) + emitter (0.4 wt %)/LiF/Al.

the triplet exciton population on the emitter and the triplet-polaron quenching (TPQ), which could explain device degradation (43–45).

To confine the high-energy excitons of a pure blue emitter that uses triplet excitons, the host or the sensitizer must have a higher triplet energy than the emitter (20). In addition, we use exciplex host to have low-efficiency roll-off and broad recombination zone compared to single host system (46). Moreover, the excitons generated in the exciplex host should be transferred to both the singlet state of the emitter or PS through Förster energy transfer. It is desirable for the exciplex host to have a short exciton lifetime and high photoluminescence quantum yield to prevent Dexter energy transfer from the triplet state of the exciplex host to the triplet state of the final TADF emitter.

The stable exciplex host, PS, and TBE are important materials for the sensitizing system. Furthermore, preferably, efficient Förster energy transfer, rather than Dexter energy transfer, must occur into TBE. Therefore, we selected a host and PS that were recently reported to exhibit extremely high device performance (47). The exciplex host, composed of 9-(3-(triphenylsilyl)phenyl)-9H-3,9'-bicarbazole (SiCzCz) and 9,9'-(6-(3-(triphenylsilyl)phenyl)-1,3,5-triazine-2,4-diyl)bis(9H-carbazole) (SiTrzCz2), was used: SiCzCz for the hole transport (HT)-type host and SiTrzCz2 for the electron transport (ET)-type host (for more information, please refer to the “Synthesis and properties of host materials” section in the Supplementary Materials and fig. S16). The bicarbazole donor unit was introduced in SiCzCz to induce a shallower HOMO level compared to that of the mono-carbazole analog, reducing the hole injection barrier between the adjacent HT layer and EML. In general, the ET host requires an electro-deficient group to achieve a suitable LUMO level for electron injection from the adjacent electron-transporting layer. Previous reports have confirmed the effectiveness of triazine (48–49) and cyano (50) groups as the blue exciplex host. The chemical structure of SiTrzCz2 selected here includes a carbazole unit attached to triazine, which confers a bipolar character, making it advantageous for reducing the driving voltage of the device. Both HT and ET host materials have the triphenylsilyl (TPS) group to efficiently suppress the triplet exciton quenching process of the exciplex. A bulky TPS group might maintain adequate intermolecular distance between host materials, reducing TTA (51) and TPQ (52). Moreover, the evaporated exciplex host film has a low ΔE_{ST} value (0.1 eV) and short exciton lifetime (5.4 μ s; tables S5 and S6 and figs. S17 and S18) with good

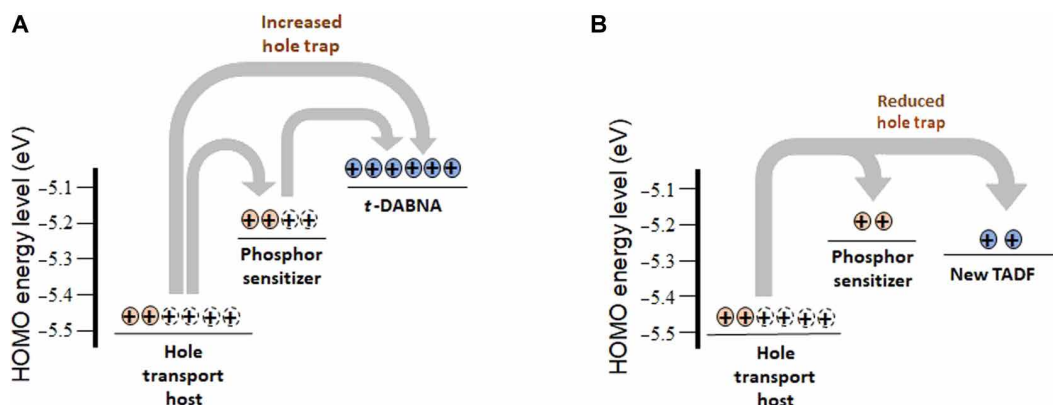


Fig. 4. Comparison of HOMO energy levels. (A) Conventional system. (B) PST system.

quantum yield (PLQY: 55%); therefore, the exciplex host can harvest triplet exciton efficiently because of its TADF characteristics (53).

Last, to allow enhanced exciton harvesting to TBE, in the sensitizing system, a sensitizer having a shorter maximum luminous wavelength than that of the TADF emitter is required. However, only a few studies have been conducted on deep-blue sensitizers with high stability, and the materials exhibiting long operational lifetime characteristics mostly have red-shifted wavelength. The use of sensitizing materials with low emission energy levels is limited because of the spectral overlap with the emitter. If the spectral overlap is small, the probability of Förster energy transfer is lowered, and device efficiency reduction is inevitable. The phosphor material, PtON-TBBI, selected here has a short PL wavelength of 454 nm and a narrow FWHM of 24 nm with excellent material stability (see figs. S19 to S25 and table S3). Cyclometalated tetradentate Pt(II) complexes with *N*-heterocyclic carbene ligands exhibit narrow FWHM because of the substantial ligand-centered electrophosphorescence. PtON-TBBI has an *N*-3,5-di-*tert*-butyl phenyl fragment in carbene that allows a strong bond formation with Pt-C_{carbene} and its modulation and facilitates the effective electron donation from the benzimidazolium

carbene to the metal center. Therefore, PtON-TBBI can serve as a stable sensitizer in the proposed sensitizing system, resulting in the acceleration of the Förster energy transfer from the T₁ of the PS to the S₁ of TBE.

Device performance

The PST system of indium tin oxide (ITO)/1,4,5,8,9,11-Hexaazatriphenylenehexacarbonitrile (HAT-CN) (10 nm)/N-([1,1'-biphenyl]-4-yl)-9,9-dimethyl-N-(4-(9-phenyl-9H-carbazol-3-yl)phenyl)-9H-fluoren-2-amine (60 nm)/SiCzCz (5 nm)/SiCzCz:SiTrzCz₂ + PS + TBEs (EML 30 nm)/2SiTrzPh (5 nm)/2SiTrzPh:Liq (5:5, 31 nm)/LiF (1.5 nm)/Al (80 nm) was fabricated; the structure is shown in Fig. 5A. BCFN and mSiTrz were introduced on the basis of previous reports (see fig. S26) (54). The EML comprised PS (PtON-TBBI) and TBEs (*t*-DABNA, TBE01, and TBE02) doped onto the exciplex host (SiCzCz:SiTrzCz₂ = 65:35%) with a doping concentrations of 13 weight % (wt %) PS and 0.4 wt % TBEs (the bottom-emissive device) or 1.0 wt % TBEs (the top-emissive device). Device 1 consisted of the exciplex host with only the PS, device 2 comprised the exciplex host with the PS and *t*-DABNA, device 3 was made up

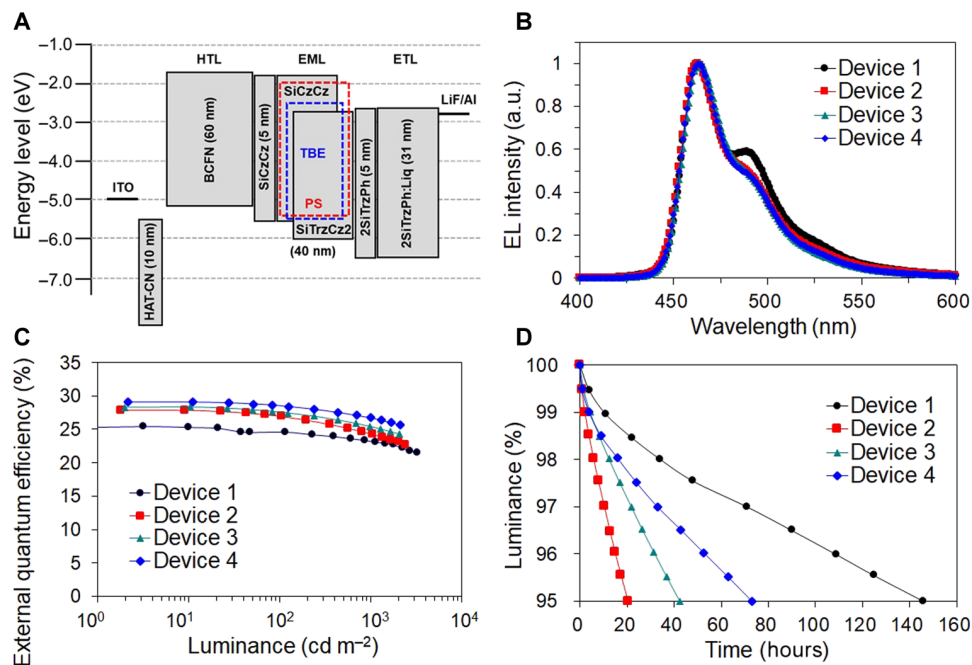


Fig. 5. OLED characteristics of the bottom-emissive devices. (A) Energy level diagram for PST-OLEDs. (B) EL spectra, (C) external EL quantum efficiency versus luminance plots, and (D) luminance versus time plots for the following devices: PS only, PtON-TBBI (13 wt %); device 1, PtON-TBBI (13 wt %) + *t*-DABNA (0.4 wt %); device 2, PtON-TBBI (13 wt %) + TBE1 (0.4 wt %); device 3, PtON-TBBI (13 wt %) + TBE2 (0.4 wt %); device 4.

Table 2. Bottom-emissive device performances of TBEs with same host and PS at 1000 nit. All lifetimes displayed here are averaged value for three sample. SD of devices 1, 2, and 3 are 0.5, 0.7, and 0.5 hours, respectively.

Bottom-emissive device	Voltage (V)	CE (cd A ⁻¹)	CIE-y	EQE (%)	LT ₉₅ (hours)	Roll-off (%)
Device 2	5.6	26.2	0.171	23.7	19.8	17.7
Device 3	5.6	27.1	0.165	25.4	42.3	12.4
Device 4	5.5	27.7	0.165	25.8	72.9	11.4
Reference (10)	4.2	36.0	0.200	24.0	11.0	–

of the exciplex host with the PS and TBE01, and device 4 consisted of the exciplex host with the PS and TBE02. The performances of these devices were evaluated. Figure 5B shows the electroluminescence (EL) spectrum for each bottom-emissive device. The PST devices have a relatively larger spectral width than TBEs because a part of emission is originated from the sensitizer. For example, emission spectrum of the device 4 exhibits similar emitter-to-sensitizer emission ratio of 55:45% (fig. S27.). Compared to device 1, the device manufactured by coevaporating the PS and TBEs, *t*-DABNA, TBE01, and TBE02 showed a decreased FWHM and improved color purity and current efficiency. Figure 5 (C and D) and Table 2 show the differences among devices 2, 3, and 4; these data help to clearly identify how the improvement of the TADF emitter affects the characteristics of the device. EQE and device lifetime at 1000 cd m⁻² of devices 2, 3, and 4 were 23.7% and 19.8 hours, 25.4% and 42.3 hours, and 25.8% and 72.9 hours in the bottom-emissive device, respectively. The PST system based on devices 3 and 4 exhibited extremely improved operational lifetimes that were 2.1 and 3.7 times higher than that of device 2 (conventional system) in the bottom-emissive device, respectively. Furthermore, the lifetime of device 4 is 6.6 times higher than that of previously reported device (24). Reduction of efficiency roll-off according to decrease of decay lifetime reflects mitigating of TPQ or TTA during device operation (Fig. 5C and Table 2). Material stability of the final emitters does not seem to be responsible for lifetime differences of PST devices examined here. Electrochemical and photochemical stability is not matching with device lifetime as explained in figs. S28 to S30. The advantage of the PST system is highlighted by the result of the top-emissive device (Fig. 6 and Table 3). The current efficiency calibrated by the Commission

Internationale de L'Eclairage (CIE)-y color coordinate, CIE-y, and the device lifetime of devices 1, 2, 3, and 4 were 301.0 cd A⁻¹ CIE-y⁻¹, 0.069, and 547.8 hours (LT50: an operational lifetime to 50% initial luminance); 320.9 cd A⁻¹ CIE-y⁻¹, 0.051, and 135.2 hours; 387.2 cd A⁻¹ CIE-y⁻¹, 0.064, and 290.6 hours; and 441.4 cd A⁻¹ CIE-y⁻¹, 0.058, and 681.5 hours in the top-emissive device, respectively. The current density for the top-emissive device lifetime evaluation was calculated by considering the blue CIE-y to achieve the white color coordinate (0.298 and 0.318). These results indicate the optimal device performance reported to date for blue OLEDs.

DISCUSSION

We demonstrated a well-designed blue TADF OLED device using the exciplex host and PS. The exciplex host, PS, and TADF as a final emitter were optimally selected to create a near-ideal environment to suppress the triplet exciton- and polaron-initiated degradation processes while maximizing exciton utilization.

A boron-derivative MR-type TADF emitter was designed to achieve high color purity, high efficiency, and long operational lifetime. The TBE with a narrow FWHM, high PLQY, and small Stokes' shift featured the following four characteristics: (i) TBE exhibited a high molar extinction coefficient for efficient Förster energy transfer via a large spectral overlap between the TBE and PS. The Förster radii of TBE increased from 3.6 nm (*t*-DABNA) to 4.5 nm (TBE02) on adding carbazole derivatives. The spectral comparison of these emitters indicates that absorbance is directly associated with the electron-rich carbazole moieties originating from the strengthened MR effect of the B-N-containing core through increased oscillator strength

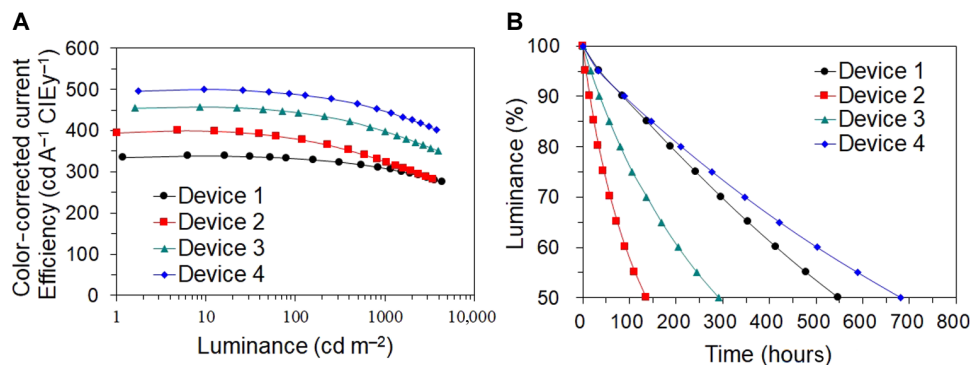


Fig. 6. OLED characteristics of the top-emissive devices. (A) Color coordinate-corrected current efficiency versus luminance plots and (B) luminance versus time plots for the following devices: PS only, PtON-TBBI(13 wt %); device 1, PtON-TBBI(13 wt %) + *t*-DABNA(1.0 wt %); device 2, PtON-TBBI (13 wt %) + TBE1(1.0 wt %); device 3, PtON-TBBI (13 wt %) + TBE2 (1.0 wt %); device 4.

Table 3. Top-emissive device performances of the TBEs with same host and PS. All device lifetimes displayed here are averaged value for three samples. SD of devices 1, 2, and 3 are 0.3, 0.2, and 1.7 hours, respectively.

Device	Voltage (V)	EQE (%)	CIE-y	CE (cd A ⁻¹ y ⁻¹)	LT ₉₅ (hours)	LT ₅₀ (hours)	Luminance* (cd m ⁻²)
Device 1	6.5	18.9	0.069	301.0	35.8	547	1527
Device 2	6.6	18.4	0.051	320.9	6.2	135.2	1113
Device 3	6.0	24.2	0.064	387.2	16.3	290.6	1399
Device 4	5.6	26.6	0.058	441.4	33.3	681.5	1260

*Measurement luminance condition.

between HOMO and LUMO (table S2). (ii) Small ΔE_{ST} between T_1 and S_1 of the TBE facilitates k_{TISC} from the triplet to S_1 . (iii) Triplet spin density shows that carbazole moieties can work as a spacer for interrupting Dexter energy transfer from nearby molecules into the emitters. (iv) The E_{HOMO} and E_{LUMO} levels of TBE01 and TBE02 having carbazole moieties are deeper than those of *t*-DABNA because the inductive withdrawing effect is dominant owing to the high electronegativity of the nitrogen atom of the carbazole unit. The hole-only devices show the subsequent increase of hole current according to the HOMO level. HOMO energy of the TBE was similar to that of the host (or the PS), which reduces the number of triplet excitons and polarons on the TBE generated by direct hole trapping.

The exciplex host, which is composed of SiCzCz as the HT host and SiTrzCz₂ as the ET host, has an energy level of 3.02 eV, which is sufficient to transfer energy to the PS. Simultaneously, the exciplex host has a low ΔE_{ST} of 0.1 eV with a short exciton lifetime of 5.4 μ s and a high PLQY of 0.55. Owing to this TADF characteristic, the exciplex host could maximize triplet exciton harvesting. PtON-TBBI exhibiting a narrow FWHM and excellent stability was implemented as a PS. Its suitable photocharacteristics enhanced Förster energy transfer from the triplet state of the sensitizer to the singlet state of the TADF emitter, resulting in low triplet exciton density in the EML.

Controlling the number of the triplet excitons and polarons generated on the TBEs facilitated the improvement of the operational lifetime by 6.6 times longer than that of the previously reported in the bottom-emitting OLEDs. We achieved state-of-the-art device performances with a device lifetime of 72.9 hours (LT_{95}) at 1000 $cd\ m^{-2}$ and an EQE of 25.8% in the bottom-emitting OLEDs and 681 hours (LT_{50}) at 1260 $cd\ m^{-2}$, a color coordinate-corrected current efficiency of 441 $cd\ A^{-1}\ CIE\ y^{-1}$, and Commission Internationale de L'Éclairage chromaticity coordinate y of 0.058 in the top-emitting OLEDs.

MATERIALS AND METHODS

Bottom-emissive OLEDs incorporating the PST system were fabricated through a configuration of ITO/BCFN:HAT-CN (100 Å)/BCFN (600 Å)/SiCzCz (50 Å)/SiCzCz:SiTrzCz₂ + PS + TBE (300 Å, 13% + 0.4%)/2SiTrzPh (50 Å)/2SiTrzPh:LiQ (310 Å)/LiF (15 Å)/Al (1000 Å). Top-emissive OLEDs incorporating the EF system were fabricated with a configuration of ITO/BCFN:HAT-CN (100 Å)/BCFN (1000 Å)/SiCzCz (50 Å)/SiCzCz:SiTrzCz₂ + PS + TBE (400 Å, 13% + 1.0%)/2SiTrzPh (50 Å)/2SiTrzPh:LiQ (310 Å)/Yb (15 Å)/Ag:Mg (120 Å)/capping layer (CPL). The structure of the EL device is shown in Fig. 5A. On the ITO substrate, p-doped BCFN was first deposited as a hole-injecting material. A hole-transporting material, BCFN, and the exciplex host doped with 13% of the PS with TBE and 2SiTrzPh:LiQ as the blue-emitting and mixed layers as an electron-transporting material, respectively, were sequentially deposited, followed by deposition of Yb, AgMg as the cathode, and CPL as the capping layer. Thereafter, the devices were encapsulated with a thin glass plate epoxy adhesive.

All chemicals were purchased from Sigma-Aldrich Co., Tokyo Chemical Industry Co., or Strem Chemicals Inc. and were used without further purification. The ¹H NMR and ¹³C NMR spectra were recorded on a Bruker ASCEND 500 instrument at 500 MHz using CDCl₃ as the solvent.

Liquid chromatography–mass spectrometry (LC–MS)–ion trap–time of flight data were recorded on a Thermo Fisher Scientific

Ultimate 3000 spectrometer. The following LC–MS conditions were used: acetonitrile and methanol as mobile phase solvents, a flow rate of 0.1 $ml\ min^{-1}$, anhydrous tetrahydrofuran (THF) as the sampling solvent, and the ACQUITY CSH C18 column (1.7 μ m, 2.1 mm by 100 mm, Waters). Heated electrospray ionization was coupled with MS.

High-resolution MS was conducted on the LTQ Orbitrap Elite system (Thermo Fisher Scientific, USA) equipped with tandem ion trap and Orbitrap systems and coupled with an ultrahigh pressure liquid chromatography device. After the sample was separated on the analysis column (Symmetry C18 column, 300 Å, 3.5 μ m, 4.6 mm by 150 mm, Waters) using acetonitrile as an eluent in the absence of additional acid at 45°C oven temperature, atmospheric pressure chemical ionization was conducted at the ionization source at 380°C [sheath gas flow rate, 35 arbitrary; discharge current, 4 μ A; S-lens radio frequency (RF) level, 50]. The MS scans were acquired at an Orbitrap resolution of 120,000 for mass/charge ratio ranging from 50 to 2000.

UV-vis spectra were obtained on a Shimadzu UV-1800 system, and the PL spectra for the solution states were achieved on a Horiba FluoroMax instrument. The UV-vis absorption and room temperature PL emission spectra were obtained using a dilute toluene solution (1×10^{-5} and 1×10^{-6} M, respectively), whereas the triplet energy values were recorded using a dilute THF solution (1×10^{-5} M, 77 K) after a delay of 1 μ s.

The energy levels were measured using DPV. Each material was dissolved in anhydrous *N,N*-dimethylformamide or dichloromethane with 0.1 M tetrabutylammonium hexafluorophosphate as an electrolyte to measure the oxidation data used to estimate energy levels of the HOMO. A platinum rod and platinum wire were used as the working and counter electrodes, respectively, and Ag/AgNO₃ was used as the pseudo reference electrode. All solutions were purged with nitrogen for 10 min before each experiment.

The NMR spectra (¹H and ¹³C) were recorded on a Bruker Advance 500 MHz spectrometer. The ¹H and ¹³C chemical shifts were reported as δ in units of parts per million, referenced to the residual solvent. Splitting patterns are denoted as singlet (s), doublet (d), triplet (t), quartet (q), multiplet (m), and broad (br). DFT simulations were performed using the B3LYP functional and 6-311G** basis set for TBE01, TBE02, and *t*-DABNA to investigate the sub-electronic energy levels and intramolecular electron orbital distributions (see fig. S12.).

SUPPLEMENTARY MATERIALS

Supplementary material for this article is available at <https://science.org/doi/10.1126/sciadv.abq1641>

REFERENCES AND NOTES

- H. Uoyama, K. Goushi, K. Shizu, H. Nomura, C. Adachi, Highly efficient organic light-emitting diodes from delayed fluorescence. *Nature* **492**, 234–238 (2012).
- A. Endo, K. Sato, K. Yoshimura, T. Kai, A. Kawada, H. Miyazaki, C. Adachi, Efficient up-conversion of triplet excitons into a singlet state and its application for organic light emitting diodes. *Appl. Phys. Lett.* **98**, 083302 (2011).
- M. A. Baldo, D. F. O'Brien, Y. You, A. Shoustikov, S. Sibley, M. E. Thompson, S. R. Forrest, Highly efficient phosphorescent emission from organic electroluminescent devices. *Nature* **395**, 151–154 (1998).
- S. Reineke, F. Lindner, G. Schwartz, N. Seidler, K. Walser, B. Lüssem, K. Leo, White organic light-emitting diodes with fluorescent tube efficiency. *Nature* **459**, 234–238 (2009).
- T. Fleetham, G. Li, J. Li, Phosphorescent Pt(II) and Pd(II) complexes for efficient, high-color-quality, and stable OLEDs. *Adv. Mater.* **29**, 1601861 (2017).
- P. K. Samanta, D. Kim, V. Coropceanu, J.-L. Brédas, Up-conversion intersystem crossing rates in organic emitters for thermally activated delayed fluorescence: Impact of the nature of singlet vs triplet excited states. *J. Am. Chem. Soc.* **139**, 4042–4051 (2017).

7. J. Gibson, A. P. Monkman, T. J. Penfold, The importance of vibronic coupling for efficient reverse intersystem crossing in thermally activated delayed fluorescence molecules. *ChemPhysChem* **17**, 2956–2961 (2016).
8. C. M. Marian, Mechanism of the triplet-to-singlet upconversion in the assistant dopant ACRXTN. *J. Phys. Chem. C* **120**, 3715–3721 (2016).
9. J. U. Kim, I. S. Park, C. Y. Chan, M. Tanaka, Y. Tsuchiya, H. Nakanotani, C. Adachi, Nanosecond-time-scale delayed fluorescence molecule for deep-blue OLEDs with small efficiency rolloff. *Nat. Commun.* **11**, 1765 (2020).
10. I. S. Park, H. Min, T. Yasuda, Ultrafast triplet-singlet exciton interconversion in narrowband blue organoboron emitters doped with heavy chalcogens. *Angew. Chem. Int. Ed.* **61**, e202205684 (2022).
11. Q. Zhang, J. Li, K. Shizu, S. Huang, S. Hirata, H. Miyazaki, C. Adachi, Design of efficient thermally activated delayed fluorescence materials for pure blue organic light emitting diodes. *J. Am. Chem. Soc.* **134**, 14706–14709 (2012).
12. I. S. Park, K. Matsuo, N. Aizawa, T. Yasuda, High-performance dibenzoheteraborin-based thermally activated delayed fluorescence emitters: Molecular architectonics for concurrently achieving narrowband emission and efficient triplet-singlet spin conversion. *Adv. Fun. Mat.* **28**, 1802031 (2018).
13. T. Hatakeyama, K. Shiren, K. Nakajima, S. Nomura, S. Nakasuka, K. Kinoshita, J. Ni, Y. Ono, T. Ikuta, Ultrapure blue thermally activated delayed fluorescence molecules: Efficient HOMO-LUMO separation by the multiple resonance effect. *Adv. Mater.* **28**, 2777–2781 (2016).
14. K. Masui, S. Oda, K. Yoshimura, K. Nakajima, N. Yasuda, T. Hatakeyama, One-shot multiple borylation toward BN-doped nanographenes. *J. Am. Chem. Soc.* **140**, 1195–1198 (2018).
15. Y. Kondo, K. Yoshimura, S. Kitera, H. Nishi, S. Oda, H. Gotoh, Y. Sasada, M. Yanai, T. Hatakeyama, Narrowband deep-blue organic light-emitting diode featuring an organoboron-based emitter. *Nat. Photon.* **13**, 678–682 (2019).
16. S. M. Suresh, E. Duda, D. Hall, Z. Yao, S. Bagnich, A. M. Z. Slawin, H. Bässler, D. Beljonne, M. Buck, Y. Olivier, A. Köhler, E. Zysman-Colman, A deep blue B,N-doped heptacene emitter that shows both thermally activated delayed fluorescence and delayed fluorescence by triplet-triplet annihilation. *J. Am. Chem. Soc.* **142**, 6588–6599 (2020).
17. X. Liang, Z.-P. Yan, H.-B. Han, Z.-G. Wu, Y.-X. Zheng, H. Meng, J.-L. Zuo, W. Huang, Peripheral amplification of multi-resonance induced thermally activated delayed fluorescence for highly efficient OLEDs. *Angew. Chem. Int. Ed.* **57**, 11316–11320 (2018).
18. S. H. Han, J. H. Jeong, J. W. Yoo, J. Y. Lee, Ideal blue thermally activated delayed fluorescence emission assisted by a thermally activated delayed fluorescence assistant dopant through a fast reverse intersystem crossing mediated cascade energy transfer process. *J. Mater. Chem. C* **7**, 3082–3089 (2019).
19. M. Yang, I. S. Park, T. Yasuda, Full-color, narrowband, and high-efficiency electroluminescence from boron and carbazole embedded polycyclic heteroaromatics. *J. Am. Chem. Soc.* **142**, 19468–19472 (2020).
20. M. A. Baldo, M. E. Thompson, S. R. Forrest, High-efficiency fluorescent organic light-emitting devices using a phosphorescent sensitizer. *Nature* **403**, 750–753 (2000).
21. H. Nakanotani, T. Higuchi, T. Furukawa, K. Masui, K. Morimoto, M. Numata, H. Tanaka, Y. Sagara, T. Yasuda, C. Adachi, High-efficiency organic light-emitting diodes with fluorescent emitters. *Nat. Commun.* **5**, 4016 (2014).
22. K. H. Lee, J. Y. Lee, Phosphor sensitized thermally activated delayed fluorescence organic light-emitting diodes with ideal deep blue device performances. *J. Mat. Chem. C* **7**, 85621–88568 (2019).
23. D. Zhang, X. Song, A. J. Gillett, B. H. Drummond, S. T. E. Jones, G. Li, H. He, M. Cai, D. Credgington, L. Duan, Efficient and stable deep-blue fluorescent organic light-emitting diodes employing a sensitizer with fast triplet upconversion. *Adv. Mater.* **32**, 1908355 (2020).
24. C. Y. Chan, M. Tanaka, Y. T. Lee, Y. W. Wong, H. Nakanotani, T. Hatakeyama, C. Adachi, Stable pure-blue hyperfluorescence organic light-emitting diodes with high-efficiency and narrow emission. *Nat. Photon.* **15**, 203–207 (2021).
25. S. O. Jeon, K. H. Lee, J. S. Kim, S. G. Ihn, Y. S. Chung, J. W. Kim, H. S. Lee, S. H. Kim, H. H. Choi, J. Y. Lee, High-efficiency, long-lifetime deep-blue organic light-emitting diodes. *Nat. Photon.* **15**, 208–215 (2021).
26. W. J. Chung, K. H. Lee, M. N. Jung, K. M. Lee, H. C. Park, M. S. Eum, J. Y. Lee, Over 30 000 h device lifetime in deep blue organic light-emitting diodes with y color coordinate of 0.086 and current efficiency of 37.0 cd A⁻¹. *Adv. Optical Mater.* **9**, 2100203 (2021).
27. S. H. Nam, J. W. Kim, H. J. Bae, Y. M. Maruyama, D. U. Jeong, J. H. Kim, J. S. Kim, W. J. Son, H. I. Jeong, J. S. Lee, S. G. Ihn, H. H. Choi, Improved efficiency and lifetime of deep-blue hyperfluorescent organic light-emitting diode using Pt(II) complex as phosphorescent sensitizer. *Adv. Sci.* **8**, 2100586 (2021).
28. L. Paterson, A. Mondal, P. Heimel, R. Lovrincic, F. May, C. Lennartz, D. Andrienko, Perspectives of unicolor phosphor-sensitized fluorescence. *Adv. Electron. Mater.* **5**, 1900646 (2019).
29. P. Heimel, A. Mondal, F. May, W. Kowalsky, C. Lennartz, D. Andrienko, R. Lovrincic, Unicolor phosphor-sensitized fluorescence for efficient and stable blue OLEDs. *Nat. Commun.* **9**, 4990 (2018).
30. H. G. Kim, H. Shin, Y. H. Ha, R. Kim, S. K. Kwon, Y. H. Kim, J. J. Kim, Triplet harvesting by a fluorescent emitter using a phosphorescent sensitizer for blue organic-light-emitting diodes. *ACS Appl. Mater. Interfaces* **11**, 26–30 (2019).
31. D. Zhang, L. Duan, TADF sensitization targets deep-blue. *Nat. Photon.* **15**, 173–174 (2021).
32. S. E. Braslavsky, E. Fron, H. B. Rodríguez, E. S. Roman, G. D. Scholes, G. Schweitzer, B. Valeur, J. Wirz, Pitfalls and limitations in the practical use of Förster's theory of resonance energy transfer. *Photochem. Photobiol. Sci.* **7**, 1444–1448 (2008).
33. H. Kuhn, Classical aspects of energy transfer in molecular systems. *J. Chem. Phys.* **53**, 101–108 (1970).
34. K. Masui, H. Nakanotani, C. Adachi, Analysis of exciton annihilation in high-efficiency sky-blue organic light-emitting diodes with thermally activated delayed fluorescence. *Org. Electron.* **14**, 2721–2726 (2013).
35. M. Cai, D. Zhang, J. Xu, X. Hong, C. Zhao, X. Song, Y. Qiu, H. Kaji, L. Duan, Unveiling the role of langevin and trap-assisted recombination in long lifespan OLEDs employing thermally activated delayed fluorophores. *ACS Appl. Mater. Interfaces* **11**, 1096–1108 (2019).
36. J. H. Lee, S. Lee, S. J. Yoo, K. H. Kim, J. J. Kim, Langevin and trap-assisted recombination in phosphorescent organic light emitting diodes. *Adv. Funct. Mater.* **24**, 4681–4688 (2014).
37. D. Zhang, X. Song, M. Cai, H. Kaji, L. Duan, Versatile indolocarbazole-isomer derivatives as highly emissive emitters and ideal hosts for thermally activated delayed fluorescent OLEDs with alleviated efficiency roll-off. *Adv. Mater.* **30**, 1705406 (2018).
38. D. L. Dexter, A theory of sensitized luminescence in solids. *J. Chem. Phys.* **21**, 836–850 (1953).
39. Y. Zhang, S. R. Forrest, Triplet diffusion leads to triplet-triplet annihilation in organic phosphorescent emitters. *Chem. Phys. Lett.* **590**, 106–110 (2013).
40. H. S. Shin, N. Tsuyoshi, J. Y. Lee, E. D. Kim, C. W. Chu, 21-3: Unveiling the degradation mechanism of phosphor-sensitized blue thermally activated delayed fluorescence OLEDs. *SID Digest* **52**, 257–260 (2021).
41. D. -G. Ha, J. Tjepelt, M. A. Fusella, M. S. Weaver, J. J. Brown, M. Einzinger, M. C. Sherrott, T. V. Voorhis, N. J. Thompson, M. A. Baldo, Dominance of exciton lifetime in the stability of phosphorescent dyes. *Adv. Opt. Mater.* **15**, 1901048 (2019).
42. D. Zhang, X. Song, M. Cai, L. Duan, Blocking energy-loss pathways for ideal fluorescent organic light-emitting diodes with thermally activated delayed fluorescent sensitizers. *Adv. Mater.* **30**, 1705250 (2018).
43. Y. Lee, C. Chan, M. Tanaka, M. Mamada, U. Balijapalli, Y. Tsuchiya, H. Nakanotani, T. Hatakeyama, C. Adachi, Investigating HOMO energy levels of terminal emitters for realizing high-brightness and stable TADF-assisted fluorescence organic light-emitting diodes. *Adv. Electron. Mater.* **7**, 2001090 (2021).
44. Y. K. Moon, H. J. Jang, S. Hwang, S. Kang, S. Kim, J. Oh, S. Lee, D. Kim, J. Y. Lee, Y. You, Modelling electron-transfer degradation of organic light-emitting devices. *Adv. Mat.* **33**, 2003832 (2021).
45. N. C. Giebink, B. W. D'Andrade, M. S. Weaver, J. J. Brown, S. R. Forrest, Direct evidence for degradation of polaron excited states in organic light emitting diodes. *J. Appl. Phys.* **105**, 124514 (2009).
46. Q. Wang, Q. S. Tian, Y. L. Zhang, X. Tang, L. S. Liao, High-efficiency organic light-emitting diodes with exciplex hosts. *J. Mat. Chem. C* **7**, 11329–11360 (2019).
47. J. Sun, H. Ahn, S. Kang, S. -B. Ko, D. Song, H. A. Um, S. Kim, Y. Lee, P. Jeon, S. -H. Hwang, Y. You, C. Chu, S. Kim, Exceptionally stable blue phosphorescent organic light-emitting diodes. *Nat. Photon.* **16**, 212–218 (2022).
48. K. J. Kim, K. M. Hwang, H. Lee, S. Kang, S. -B. Ko, M. -S. Eum, Y. K. Kim, T. Kim, Extremely superb efficiency and lifetime of deep blue phosphorescent OLEDs by introducing a hypsochromic emissive intermolecular complex (HEIC) with a negligibly small ΔE_{ST} and fast reverse intersystem crossing rate. *J. Mater. Chem. C* **9**, 4029–4038 (2021).
49. M. Jung, K. H. Lee, J. Y. Lee, T. Kim, A bipolar host based high triplet energy electroplex for an over 10 000 h lifetime in pure blue phosphorescent organic light-emitting diodes. *Mater. Horiz.* **7**, 559–565 (2020).
50. S. K. Shin, S. H. Han, J. Y. Lee, High triplet energy exciplex host derived from a CN modified carbazole based n-type host for improved efficiency and lifetime in blue phosphorescent organic light-emitting diodes. *J. Mater. Chem. C* **6**, 10308–10314 (2018).
51. S. Reineke, G. Schwartz, K. Walsler, K. Leo, Reduced efficiency roll-off in phosphorescent organic light emitting diodes by suppression of triplet-triplet annihilation. *Appl. Phys. Lett.* **91**, 123508 (2007).
52. N. C. Giebink, B. W. D'andrade, M. S. Weaver, P. B. Mackenzie, J. J. Brown, M. E. Thompson, S. R. Forrest, Intrinsic luminance loss in phosphorescent small-molecule organic light emitting devices due to bimolecular annihilation reactions. *J. Appl. Phys.* **103**, 044509 (2008).
53. T. B. Nguyen, H. Nakanotani, T. Hatakeyama, C. Adachi, The role of reverse intersystem crossing using a TADF-type acceptor molecule on the device stability of exciplex-based organic light-emitting diodes. *Adv. Mater.* **32**, 1906614 (2020).
54. K. H. Choi, K. H. Lee, J. Y. Lee, T. Kim, Simultaneous achievement of high efficiency and long lifetime in deep blue phosphorescent organic light-emitting diodes. *Adv. Opt. Mater.* **7**, 1901374 (2019).

Acknowledgments: This work was supported by Samsung Display. **Funding:** We acknowledge that we received no funding in support of this research. **Author contributions:** E.K., J.P., M.J., H.S., H.A., Seran K., J.L., and J.Y.L. wrote the manuscript. C.C. and Sunghan K. supervised the project. E.K. and M.J. optimized the device structures of the bottom- and top-emissive devices. E.K., M.J., H.S., and J.L. fabricated and analyzed the device data. H.S. and J.L. characterized the electrical and physical properties of the thin films, fabricated the devices, and analyzed the device data. J.P., J.B., and T.K. designed and characterized the TADF emitter. Seran K. performed the calculations for the TADF materials. J.S. and S.-B.K. designed and characterized the phosphor. H.A. designed and characterized the host under the supervision of S.-H.H. All authors

contributed to the discussion of this study. **Competing interests:** The authors declare that they have no competing interests. **Data and materials availability:** All data needed to evaluate the conclusions in the paper are present in the paper and/or the Supplementary Materials.

Submitted 18 April 2022

Accepted 29 August 2022

Published 14 October 2022

10.1126/sciadv.abq1641